QJEGH
Research article
*Quarterly Journal of Engineering Geology and Hydrogeology*
https://doi.org/10.1144/qjegh2024-036 | Vol. 57 | 2024 | qjegh2024-036

# The influence of earthworks construction on porewater pressures in clays and mudstones of the Lias Group

**Kevin M. Briggs[1*], Yuderka Trinidad González[2], Gerrit J. Meijer[3], Andrew Ridley[4], William Powrie[1], Simon Butler[5‡] and Nick Sartain[5]**

[1] Faculty of Engineering and the Environment, University of Southampton, University Road, Highfield, Southampton SO17 1BJ, UK
[2] Department of Civil, Construction, and Environmental Engineering, Iowa State University, Town Engineering Building, 394 Town Engineering, Ames, IA 50011, USA
[3] Department of Architecture and Civil Engineering, University of Bath, Bath BA2 7AY, UK
[4] Geotechnical Observations Ltd, 9 Avro Way, Brooklands, Weybridge KT13 0YF, UK
[5] High Speed Two (HS2) Ltd, Two Snowhill, Snow Hill Queensway, Birmingham B4 6GA, UK
KMB, 0000-0003-1738-9692; YTG, 0000-0003-3715-9712; GJM, 0000-0002-2815-5480; WP, 0000-0002-2271-0826
* Correspondence: K.Briggs@soton.ac.uk
‡ Seconded from Atkins

**Abstract:** Monitoring the changes in porewater pressure associated with the construction of earthworks can yield information on the stiffness and permeability of the ground, as well as how the natural groundwater regime might be impacted. This paper presents 3 years of porewater pressure measurements in weathered Lias Group mudstone, obtained from a trial cutting and a trial embankment constructed for the UK's High Speed Two (HS2) railway. The immediate changes in porewater pressure were small in relation to the changes in total stress imposed. This can be explained by the consolidation or swelling during the period of construction, combined with the sensitivity of very stiff clays and mudstones to a very small (0.5%) reduction in the degree of saturation. In the longer term, porewater pressures reduced across the site owing to the reduction in ground level at the trial cutting. Rates of porewater pressure change were accelerated by more permeable limestone within the ground profile reducing drainage path lengths. It was concluded that construction-induced porewater pressure changes may be smaller, and their rate of dissipation more rapid, in weathered clays and mudstones such as those of the Lias Group than in younger, more compressible clay deposits.

**Thematic collection:** This article is part of the Geo-resilience and infrastructure collection available at: https://www.lyellcollection.org/topic/collections/geo-resilience-and-infrastructure

**Received** 4 March 2024; **revised** 13 May 2024; **accepted** 14 July 2024

Porewater pressures play a fundamental role in the stability of natural and engineered (earthworks) slopes; hence, they have a huge potential to impact the georesilience of transportation infrastructure that is built on embankments, in cuttings or on sidelong natural ground. The construction of earthworks can cause changes in porewater pressure in both the short term (owing to changes in total stress associated with loading or unloading the natural ground) and in the long term (owing to changes in the equilibrium local hydrogeological groundwater regime). Monitoring these changes in porewater pressure can yield information on the stiffness and permeability of the ground, as well as how the natural groundwater regime might be impacted by the new infrastructure. Porewater pressure measurement can also inform construction in difficult or uncertain hydrogeological conditions, where knowledge of the potential for consolidation settlements or the transition from undrained to drained soil behaviour (Powrie and Roberts 1990) may be important. They can also provide baseline measurements to inform responsive construction techniques such as the Observational Method (Peck 1969; Roberts and Preene 1994; Powderham and O'Brien 2020).

There are numerous case studies in the literature describing the monitoring of porewater pressures in weathered, overconsolidated clays and mudstones during and after construction-related processes. These include construction of, and dewatering for, embankments, tunnels and deep excavations at individual sites (Vaughan and Walbancke 1973; Whittle *et al.* 1993; Powrie and Roberts 1995; Ng 1998; Richards *et al.* 2007; Roberts *et al.* 2007; Wan and Standing 2014; Lawrence *et al.* 2018*b*) and regionally (Newman 2009; Lawrence *et al.* 2018*a*). Many UK studies have focused on Paleogene and Cretaceous clay deposits in the south and east of England. However, less is known about the hydrogeology of the weathered, Jurassic clays and mudstones in central England, or their porewater pressure response to the construction of large structures such as railway cuttings and embankments.

The construction of the UK High Speed 2 (HS2) railway between London and Birmingham provided an opportunity to obtain monitoring data within and beneath earthworks constructed in a range of geological strata. This paper describes porewater pressure measurements in ground comprising weathered clays and mudstones of the Lias Group during and after earthworks construction at a site in central England. Three years of monitoring data from a trial cutting and a trial embankment, supplemented by *in situ* and laboratory test data, are used to evaluate (i) the short-term and (ii) the long-term porewater pressure changes at depth in response to the construction of earthworks at the original ground surface.

## Materials and methods

The trial cutting and embankment were located at Boddington near Wormleighton, 14 km north of Banbury, England (52° 11′ 14″ N,

© 2024 The Author(s). This is an Open Access article distributed under the terms of the Creative Commons Attribution 4.0 License (http://creativecommons.org/licenses/by/4.0/). Published by The Geological Society of London. Publishing disclaimer: https://www.lyellcollection.org/publishing-hub/publishing-ethics

1° 20′ 21″ W). Boddington is within a *c.* 18.2 km-wide outcrop of the Charmouth Mudstone Formation that is crossed by the HS2 railway between London and Birmingham (Fig. 1). Boddington is located in the East Midlands Shelf basin of the Lias Group, where the Charmouth Mudstone Formation is *c.* 100–150 m thick (Hobbs *et al.* 2012). It was formed *c.* 183–199 Myr ago in a shallow-marine environment and was subsequently overconsolidated. The formation is principally mudstone, with alternating sequences of mudstone, limestone and sandstone that result from cyclical patterns of deposition. Boddington is located to the north of a region of lowland periglaciated terrain in central and southern England (Booth *et al.* 2015), and close to the southern limit (*c.* 147 kyr ago) of the Moreton Stadial glaciation of the Late Wolstonian Substage (Gibson *et al.* 2022). It was therefore subjected to periglacial and contemporary weathering during the Quaternary Period. The mudstone has weathered to clay at shallower depths (0–11 m below ground level (bgl)), forming a gradational weathering profile from the ground surface (Briggs *et al.* 2022).

The trial cutting was constructed between 23 July 2019 and 11 December 2019 to a final depth of 13 m bgl at the centre. Aerial drone surveys were undertaken to measure the progress of the excavation at approximately weekly intervals. When finished, the cutting was *c.* 290 m long and 130 m wide at the original ground level (Fig. 2). The base of the cutting was 15 m wide, with slopes excavated to *c.* 1 (V) in 4 (H). Directly to the north and adjacent to the trial cutting, a trial embankment was constructed in stages between 7 November 2020 and 9 December 2020 using fill excavated from the trial cutting. It was *c.* 150 m long and 95 m wide at the base, with a crest width of 55 m and a slope angle of *c.* 1 (V) in 2.3 (H) (Fig. 2). The final height of the embankment was 8.2 m. It was demolished almost 2 years later in the autumn of 2022. The Oxford Canal passes 100 m to the north of the trial embankment at a low point in the local topography at *c.* 116 m above Ordnance Datum (AOD). Surface water ponding occurred within the trial cutting at Boddington in the autumn of 2019, following a wet summer and prolonged autumn rainfall in central England (Meteorological Office 2024*a*). Surface water ponding also occurred in the spring months of both 2020 and 2021, immediately after construction of the trial cutting and trial embankment, respectively. This correlates with instances of high water levels in the River Cherwell at Cropredy Bridge, 5 km south of Boddington (Environment Agency 2024).

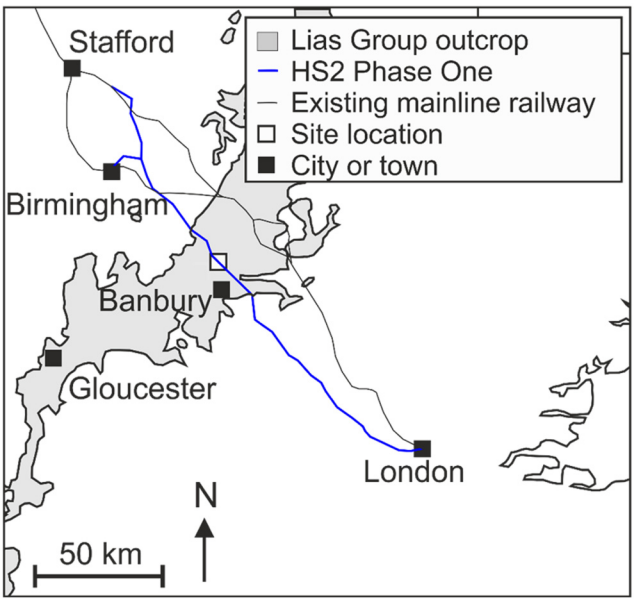


**Fig. 1.** The Boddington site is located in a mudstone outcrop of the Lias Group in central England, on the alignment of the HS2 railway between London and Birmingham.

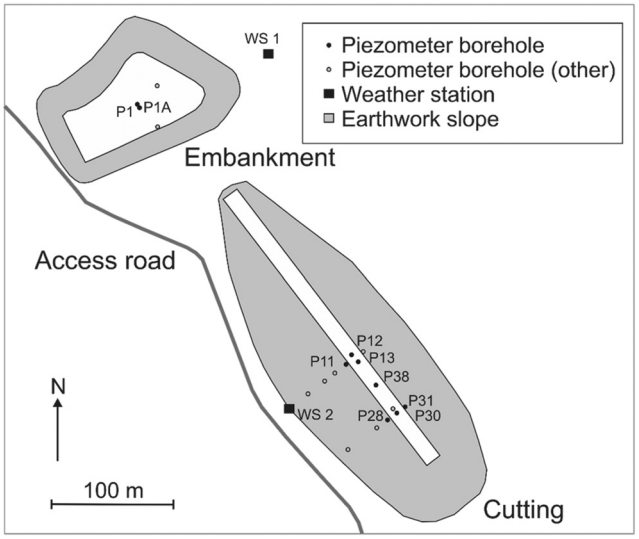


**Fig. 2.** Site plan showing the location of boreholes with piezometer installations (labelled) beneath a trial embankment and trial cutting at Boddington, near Wormleighton, England (52° 11′ 14″ N, 1° 20′ 21″ W).

A ground investigation was undertaken by commercial contractors along the full length of the HS2 alignment through the Charmouth Mudstone Formation outcrop, including at Boddington. Instruments including weather stations, piezometers, inclinometers and extensometers were installed beneath the trial cutting and the trial embankment prior to construction, and monitored during and after the construction period. The monitoring data were used to observe the heave and settlement of the trial cutting and trial embankment, respectively, to inform the design of earthworks for the HS2 railway. This study analyses only the piezometer and weather station data.

## Ground investigation

More than 40 boreholes were drilled and logged at Boddington prior to the construction of the earthworks. Samples were recovered for laboratory index testing, oedometer testing and triaxial testing. *In situ* testing was undertaken to measure the saturated hydraulic conductivity and stiffness of the ground profile.

Figure 3 shows simplified stratigraphic ground profiles beneath the trial cutting and trial embankment, as informed by the borehole strata descriptions. The ground surface at the trial cutting was located at 136 m AOD and consisted of 13 m of weathered clay overlying weathered mudstone and a *c.* 2 m-thick band of limestone (described as calcareous siltstone) at 104 m AOD (32 m bgl). Unweathered mudstone was present below 102 m AOD. The trial embankment was located downslope and to the north of the trial cutting at an elevation of 122 m AOD. At the trial embankment site, the ground profile comprised *c.* 12 m of weathered clay overlying weathered mudstone and a *c.* 2 m-thick band of limestone at 104 m AOD (18 m bgl). Again, the mudstone below 102 m AOD was unweathered. At both the trial cutting and trial embankment sites, an additional limestone stratum was identified at *c.* 84 m AOD in a limited number of boreholes. Examination of borehole logs from across the wider Charmouth Mudstone Formation outcrop showed that the limestone strata beneath Boddington dips gently (<1°) to the SE. The transition from clay to mudstone and limestone (Fig. 3) was discernible in optical borehole images from Boddington (not shown). Figure 4 shows that the moisture content (%) and plasticity index (%) of the clay and mudstone at Boddington are depth dependent. They are greatest and most variable near the surface

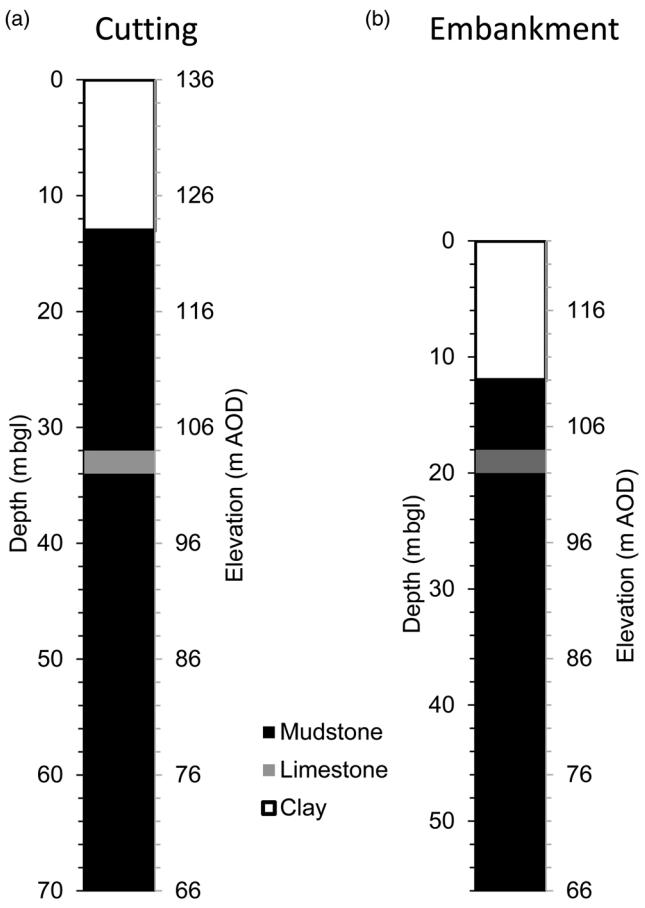


**Fig. 3.** The ground profile beneath (**a**) the trial cutting and (**b**) the trial embankment. The clay, mudstone and limestone strata are shown based on borehole logger descriptions.

(<5 m bgl) but more uniform at depth. These data are consistent with measurements in the Charmouth Mudstone Formation outcrop north of Banbury, England (Briggs *et al.* 2022).

Figure 5 shows the saturated hydraulic conductivity ($k_{sat}$) profile at Boddington, derived from tests on triaxial specimens 75–100 mm in diameter (BS EN ISO 17892-11:2019: BSI 2019), oedometer tests (BS EN ISO 17892-5:2017: BSI 2017) and *in situ* packer

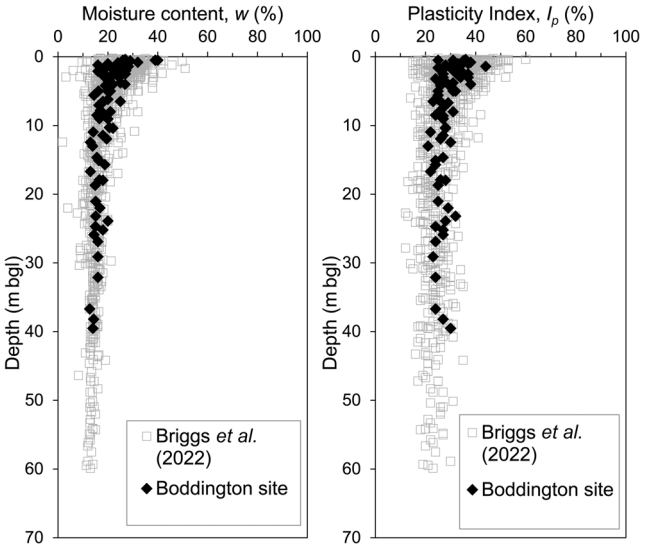


**Fig. 4.** Moisture content ($w$: %) and plasticity index ($I_p$: %) profiles based on samples obtained at Boddington and from the wider ground investigation (Briggs *et al.* 2022).

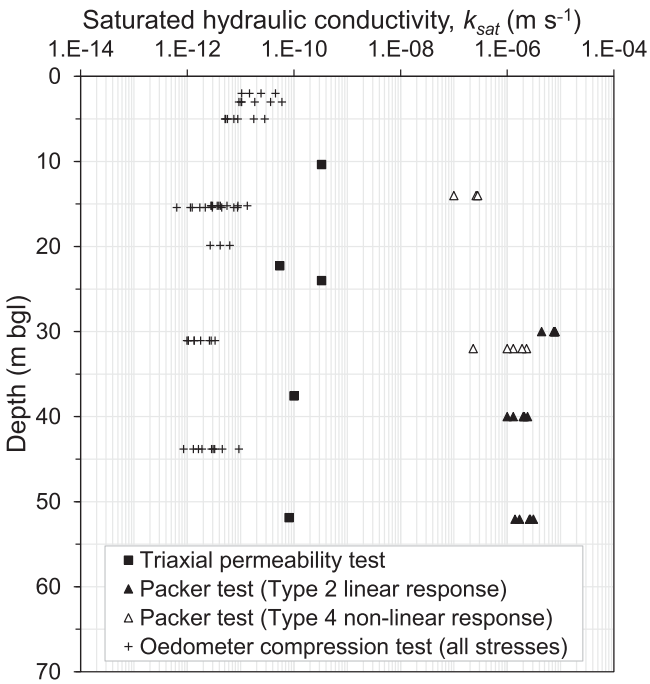


**Fig. 5.** *In situ* and laboratory measurements of saturated hydraulic conductivity ($k_{sat}$) at Boddington compared to sample or measurement depth. The oedometer compression test stages did not align consistently with *in situ* stresses, so all test stages are shown.

permeability tests (BS EN ISO 22282-3:2012: BSI 2012) using the Preene (2019) interpretation. The laboratory tests show that the saturated vertical hydraulic conductivity ($k_{v,sat}$) of the samples was between $10^{-13}$ and $10^{-10}$ m s$^{-1}$. This is within the general range for weathered clays and mudstones (Smethurst *et al.* 2006; Hobbs *et al.* 2012), although laboratory test data from larger samples (at least 250 mm in diameter) would have given a better indication of the influence of soil fabric (Rowe 1972). The *in situ* tests gave values of saturated hydraulic conductivity many orders of magnitude greater ($10^{-7}$–$10^{-6}$ m s$^{-1}$) than the laboratory tests. This is because the *in situ* tests involve substantially horizontal flow and hence are most representative of the saturated horizontal hydraulic conductivity ($k_{h,sat}$). The horizontal hydraulic conductivity of a natural deposit is usually greater than the vertical hydraulic conductivity, often by orders of magnitude if there are preferential flow pathways controlled by bedding (Powrie and Roberts 1990) or other discontinuities (Rowe 1972; Preene 2019). Neither the laboratory nor the *in situ* measurements showed any significant decrease in saturated hydraulic conductivity with depth; this is consistent with the highly overconsolidated nature of the deposit.

Figure 6 shows shear-wave velocity (m s$^{-1}$) measurements made in four boreholes (DHGEO) at Boddington by a specialist contractor for the HS2 ground investigation. Shear-wave velocities were generated by a sledgehammer striking the end of a timber sleeper at the ground surface. They were detected by a BGK-7 multi-element geophone with one vertical and six horizontal sensors, with azimuthal axes at 30° intervals. The BGK-7 multi-element geophone was pneumatically clamped in the boreholes at each successive test depth, which were at 1 m intervals. Broadly, the measurements show transitions in the shear-wave velocity profile and, by implication, in stiffness (Poulos 2022). These have been plotted by elevation so that the measurements in the deeper, less-weathered clays and mudstones from both the trial cutting and trial embankment can be compared. Figure 6 shows four zones: (i) 128–136 m AOD; (ii) 116–128 m AOD; (iii) 102–116 m AOD; and (iv) below 102 m AOD. There was a bi-linear increase in shear-wave velocity (and therefore stiffness) with depth in the clay (>123 m

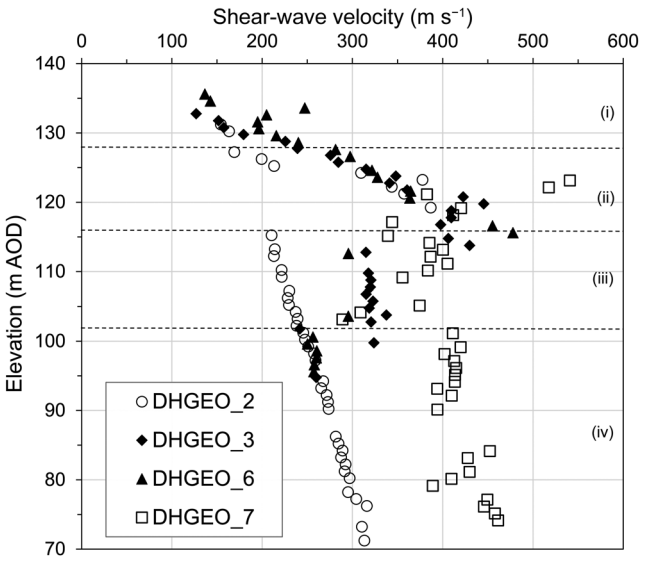


**Fig. 6.** Downhole measurements of shear-wave velocity (m $s^{-1}$) derived from downhole geophysical measurements in four boreholes (DHGEO_2, DHGEO_3, DHGEO_6 and DHGEO_7) at the trial cutting prior to excavation (adapted from Briggs *et al.* 2024). The measurements can be divided into four zones: (i) 128–136 m AOD; (ii) 116–128 m AOD; (iii) 102–116 m AOD; and (iv) below 102 m AOD.

AOD) and weathered mudstone (116–123 m AOD) in zones (i) and (ii). This corresponds to a stiffness profile dependent on *in situ* stress and the void ratio, as is typical for a clay (Vardanega and Bolton 2013; Briggs *et al.* 2024). Below 116 m AOD in zones (iii) and (iv) the measurements are more scattered and increase at a lesser rate with depth or *in situ* stress than above. This is typical of a transition from clay to rock (i.e. an unweathered, cemented mudstone). The shear-wave velocity profile did not vary at the transition between the mudstone and the limestone (102–104 m AOD). The measurements at DHGEO_2 differ from those at other locations in that they reduce to low values below 116 m AOD. This could not be explained with reference to the borehole strata descriptions or the optical borehole log, and the reason for it remains unclear.

## Piezometers

Vibrating wire piezometers and GeO flushable piezometers were installed using the fully grouted method and maintained at Boddington by a contractor to inform the design of earthworks for the HS2 railway (Fig. 2). Piezometers installed below the excavation level of the trial cutting (i.e. below 123 m AOD) and beneath the centre of the trial embankment (i.e. below the original ground surface at 122 m AOD) were selected for analysis because these locations were at the centroids of the zones of uniform unloading or loading. Piezometers located in regions of non-uniform loading, such as below the slopes of the trial cutting, above the excavated level of the cutting or close to the edge of the trial embankment, were not considered. A small number of piezometers malfunctioned and required resetting or reflushing during the monitoring period. These were also excluded from the analyses. During the installation of piezometers in borehole P1, a loss of grout through a preferential flow pathway occurred, which was accompanied by a water-level rise at a borehole downslope. The borehole then collapsed at 12 m bgl overnight. The measurements from the shallower piezometers at P1 (at 10 and 20 m bgl) were therefore considered unreliable, and those from the adjacent borehole P1A (Table 1) were used in the analyses in preference.

Details of the fully grouted piezometers installed at Boddington and selected for analysis are shown in Table 1. Geotechnical Observations Ltd GeO flushable piezometers (GeO FP) were installed above 104 m AOD at the trial cutting to allow measurement of both positive and negative porewater pressures. Geosense VWP-3000 series vibrating wire piezometers (VWP3000) were installed below 104 m AOD at the trial cutting. RST Instruments VW2100 vibrating wire piezometers (VW2100) were installed beneath the trial embankment. The GeO flushable piezometers have Geokon 4500C sensors and high air-entry (3 bar) porous filters so they can measure negative porewater pressure (suction) to −100 kPa (Ridley *et al.* 2003). The porous filters were saturated in a vacuum chamber and transported to the site in de-aired water. Each piezometer consists of a 50 mm-diameter UPVC pipe with a high air-entry porous filter at the bottom of the pipe and a sensor/valve that is screwed into place at the bottom of the pipe and sealed with an O-ring. The pipe is grouted in place and the grout acts as a secondary filter for transmitting negative porewater pressures

**Table 1.** Piezometers installed in borehole locations (BH) at Boddington and considered for analysis (Fig. 2)

| Name | BH | Type | Elevation (m AOD) | Depth (m bgl) | Start date (day/month/year) | End date (day/month/year) |
|---|---|---|---|---|---|---|
| P1_112 m* | P1 | VW2100 | 112 | 10 | 05/11/2020 | 04/10/2022 |
| P1_102 m* | P1 | VW2100 | 102 | 20 | 05/11/2020 | 04/10/2022 |
| P1_88 m | P1 | VW2100 | 88 | 34 | 05/11/2020 | 04/10/2022 |
| P1A_112 m | P1A | VW2100 | 112 | 10 | 05/11/2020 | 04/10/2022 |
| P1A_102 m | P1A | VW2100 | 102 | 20 | 05/11/2020 | 04/10/2022 |
| P11_118 m | P11 | GeO FP | 118 | 18 | 23/07/2019 | 01/01/2023 |
| P12_113 m | P12 | GeO FP | 113 | 23 | 23/07/2019 | 14/11/2022 |
| P13_120 m | P13 | GeO FP | 120 | 16 | 23/07/2019 | 14/11/2022 |
| P13_118 m | P13 | GeO FP | 118 | 18 | 23/07/2019 | 14/11/2022 |
| P28_118 m | P28 | GeO FP | 118 | 16 | 23/07/2019 | 01/01/2023 |
| P28_103 m | P28 | VWP3000 | 103 | 31 | 23/07/2019 | 01/01/2023 |
| P30_121 m | P30 | GeO FP | 121 | 14 | 23/07/2019 | 14/11/2022 |
| P30_118 m | P30 | GeO FP | 118 | 16 | 23/07/2019 | 14/11/2022 |
| P31_88 m | P31 | VWP3000 | 88 | 46 | 23/07/2019 | 01/01/2023 |
| P31_73 m | P31 | VWP3000 | 73 | 61 | 23/07/2019 | 01/01/2023 |
| P38_118 m | P38 | GeO FP | 118 | 17 | 23/07/2019 | 14/11/2022 |
| P38_103 m | P38 | VWP3000 | 103 | 32 | 23/07/2019 | 14/11/2022 |

Note: the instruments included RST Instruments VW2100 vibrating wire piezometers (VW2100), Geotechnical Observations Ltd GeO flushable piezometers (GeO FP) and Geosense VWP-3000 series vibrating wire piezometers (VWP3000). The start dates refer to the dates considered in the analyses but measurements were recorded prior to this. *Loss of grout and collapse of borehole at *c.* 12 m bgl during installation.

from the soil to the piezometer (Tarantino *et al.* 2008). According to BS EN ISO 18674-4:2020 (BSI 2020), piezometers that do not include a method of removing air (e.g. flushing tubes) should have low air-entry filters. The Geosense and RST Instruments vibrating wire piezometers were therefore fitted with low air-entry porous filters, thus making them suitable for the fully grouted installation method. Both the Geosense vibrating wire piezometers and the RST Instruments vibrating wire piezometers were assembled by joining the bodies of the piezometers and the porous filters in de-aired water before they were attached to UPVC installation pipes (facing upwards). They were then lowered into the boreholes and grouted in place using a water–cement–bentonite grout ratio of 2.0 : 1.0 : 0.3 by weight. The piezometers beneath the trial cutting were installed between January and March 2019, before excavation began in July 2019. The piezometers were installed beneath the trial embankment in October 2020, before construction began in November 2020.

Vibrating wire piezometers are normally hermetically sealed and can respond to changes in atmospheric pressure when the phreatic surface is located close to the ground surface. The measurements from all of the piezometers were examined for changes resulting from fluctuations in the ambient atmospheric pressures and adjusted as necessary. The VWP3000 and VW2100 vibrating wire piezometers (Table 1) are sealed and therefore responded to fluctuations in atmospheric pressure. Guidance in BS EN ISO 18674-4:2020 (BSI 2020) recommends adjustment using the constant ambient reference pressure at which the sensor was sealed, or using a constant reference pressure. Readings from the instruments at Boddington were therefore adjusted to give gauge pressures ($u$) relative to a constant atmospheric pressure ($u_{atm,average}$) using:

$$u = u_{measured} + u_{atm,average} - u_{atm,measured} \quad (1)$$

where $u_{measured}$ is the measured porewater pressure (kPa), $u_{atm,measured}$ is the measured atmospheric pressure at the weather station (kPa) and $u_{atm,average}$ is the average, long-term atmospheric pressure (*c.* 100 kPa). The GeO flushable piezometers measured gauge pressures (relative to atmospheric pressure) and therefore did not require adjustment.

## Weather stations

Two weather stations were installed at Boddington (Fig. 2). The weather stations recorded hourly measurements from: (i) a Campbell Scientific CS215 sensor to measure temperature (°C) and relative humidity (RH: %); (ii) a Campbell Scientific ARG100 tipping-bucket rain gauge to measure rainfall (mm $h^{-1}$); (iii) a Campbell Scientific 03002 Wind Sentry to measure wind speed (m $s^{-1}$) and direction (°); and (iv) a Campbell Scientific CS106 barometer to measure the barometric pressure (kPa). The two weather stations were located within 300 m of each other (Fig. 2) and their measurements were in close agreement.

Hourly weather station measurements were converted to daily values of minimum and maximum temperature ($T$: °C) and RH (%); mean wind speed (m $s^{-1}$) and direction (°); and daily rainfall ($R$: mm). An upper-bound indication (Smethurst *et al.* 2006) of the daily atmospheric drying from bare soil and vegetation due to potential evapotranspiration (PET: mm/day) was calculated using a simple relationship with minimal parameters (Schendel 1967), included in a sensitivity analysis of different PET models by Bormann (2011):

$$PET = 16\frac{T}{RH} \quad (2)$$

The daily rainfall and PET were summed to give annual totals and to compare relative atmospheric wetting and drying in different years. These were compared with historical weather station data from Wellesbourne (*c.* 32 km east of Boddington) and long-term average values published by the Meteorological Office (2024*b*). The daily atmospheric water balance ($B_{atm}$: mm/day) was calculated following Blight (1997) as the rainfall, $R$ (mm/day), measured at the Boddington site minus the PET (mm/day) derived from equation (2). The daily values were summed to calculate the change in $B_{atm}$ at Boddington (2019–2023) for comparison with any seasonal porewater pressure trends in the piezometer measurements.

## Total stress changes due to earthwork construction

Construction of the trial cutting at Boddington reduced the total stresses in the underlying ground and lowered the local elevation of the ground surface. Construction of the trial embankment increased the total stresses in the underlying ground. The changes in vertical, horizontal and average total stress beneath the earthworks at the end of construction were calculated at each piezometer location for comparison with the piezometer measurements. The changes in stress were calculated by superposition of the analytical equations for stress increments in an isotropic, linear elastic half-space for vertical loading and plane-strain conditions, derived by Gray (1936) and summarized in Poulos and Davis (1974). Excavation of the cutting was modelled by removing the overburden corresponding to the excavated depth (13 m bgl) across the entire half-space, then adding back the load associated with infinitely long ($b = \infty$) embankments at the locations of the cutting slopes (Fig. 7). Construction of the trial embankment was modelled by directly using the equations for increases in load associated with an embankment slope of limited crest width (Poulos and Davis 1974):

$$\Delta\sigma_z = \frac{P}{\pi}\left[\beta + \frac{x\alpha}{a} - \frac{z}{R_2^2}(x-b)\right] \quad (3)$$

$$\Delta\sigma_x = \frac{P}{\pi}\left[\beta + \frac{x\alpha}{a} - \frac{z}{R_2^2}(x-b) + \frac{2z}{a}\ln\frac{R_1}{R_0}\right] \quad (4)$$

where $\Delta\sigma_z$ is the change in vertical stress, $\Delta\sigma_x$ is the change in horizontal stress (in the vertical cross-sectional plane), $P$ is the surface load, $x$ is the horizontal location from the earthwork midpoint, $z$ is the vertical location (i.e. depth) and the remaining parameters ($a$, $b$, $\alpha$, $\beta$, $R_0$, $R_1$ and $R_2$) describe the embankment geometry (Fig. 7).

The change in average total stress ($\Delta p$) was calculated as:

$$\Delta p = \frac{1}{2}(\Delta\sigma_z + \Delta\sigma_x) \quad (5)$$

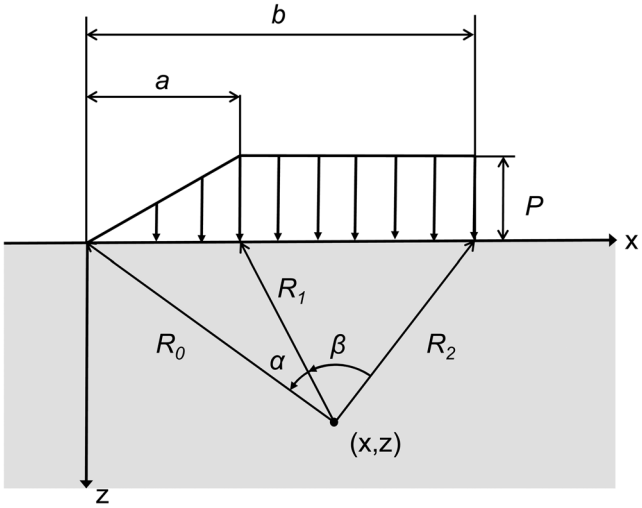


**Fig. 7.** The geometry parameters for the distributed vertical embankment loading equations described in Poulos and Davis (1974).

This assumes that the change in the intermediate principal stress $\Delta\sigma_y$ (along the direction of the earthwork) is the average of the changes in the major and minor principal stresses $\Delta\sigma_x$ and $\Delta\sigma_z$. If the soil behaviour is elastic and the porewater may be regarded as incompressible in comparison with the soil skeleton, there can be no change in average effective stress, $p'$, without a change in specific volume. Hence, in undrained conditions, the change in porewater pressure, $\Delta u$, should be equal to the change in average total stress, $\Delta p$. In other words, the Skempton (1954) $B$ value, which is derived from:

$$B = \frac{\Delta u}{\Delta p} \tag{6}$$

should be equal to unity.

### Surface drainage due to earthwork construction

Construction of the trial cutting lowered the ground level by up to 13 m. This is considerably below the depth of 0.8 m bgl, below which porewater pressures were found to be hydrostatic prior to construction (Briggs *et al.* 2022). Thus, once the excavation was complete, it provided a local sink for groundwater flow through the base and sides of the cutting, which was removed by surface drainage. This resulted in a long-term lowering of the equilibrium porewater pressures in the ground beneath the earthworks at Boddington, with a maximum reduction of 127.5 kPa at the centre of the trial cutting.

## Results and Discussion

### The site atmospheric water balance

Figure 8 shows annual cumulative totals of rainfall and PET at Boddington, compared with Met Office (2024*b*) annual long-term average (LTA) rainfall at Wellesbourne and for the Midlands. Wellesbourne is at a lower elevation and drier than Boddington. The PET is relatively constant each year, in agreement with observations at other UK earthwork sites (Smethurst *et al.* 2006; Briggs *et al.* 2016). The total annual rainfall reduced each year from 2020 to 2023 and the earthworks monitoring period was generally drier than the LTA, with the exception of the wet summer and autumn of 2019 (Met Office 2024*a*). The atmospheric water balance ($B_{atm}$) at Boddington (given by the rainfall minus the PET) increased during the winter months (September–April) – that is, the atmosphere became wetter – and reduced during the summer months (April–September) (Fig. 9).

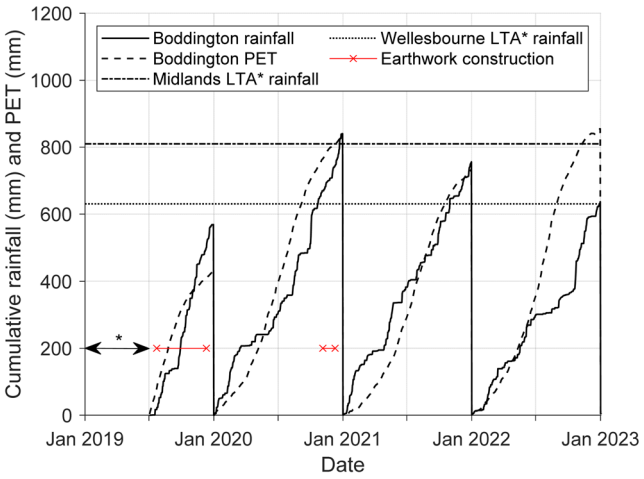


**Fig. 8.** Cumulative annual rainfall (mm) and potential evapotranspiration (PET, mm) measured at Boddington, compared to the Met Office (2024*b*) annual long-term average (LTA) rainfall totals at Wellesbourne and in the Midlands. The start and end dates for the construction of the trial cutting (2019) and trial embankment (2020) are shown in red. Note: there are no data prior to July 2019 (shown as *).

### Porewater pressure changes

Figure 9 shows changes in porewater pressure and the atmospheric water balance ($B_{atm}$) beneath the trial cutting (Fig. 9a, b) and the trial embankment (Fig. 9c) following the start of construction. The piezometers located beneath the cutting and above 104 m AOD showed rapid reductions in porewater pressures during construction, followed by gradual long-term reductions in porewater pressures of up to about 125 kPa (Fig. 9a). The piezometers beneath the cutting and below 104 m AOD also showed rapid, but more limited, reductions in porewater pressures during construction, followed by more gradual long-term reductions in porewater pressures (*c.* 25–75 kPa) than at higher elevations. There were small, seasonal variations in these porewater pressures (<5 kPa), showing a partial recovery of excess porewater pressures towards the end of the excavation period (Fig. 9b). The measurements beneath the trial embankment (Fig. 9c) show rapid increases in porewater pressures during construction, rapid decreases during removal of the embankment and long-term trends of gradual porewater pressure reductions (*c.* 25 kPa over the period), similar to those observed at greater depths beneath the cutting. There are small, seasonal variations in these porewater pressure measurements (<10 kPa) that are greatest at depths below 104 m AOD.

Figure 10 shows profiles of porewater pressure beneath the trial cutting with elevation for dates at the start of construction, at the end of construction and in the longer term. A limited number of piezometer measurements (Briggs *et al.* 2022) indicated a hydrostatic profile of porewater pressures below 0.8 m bgl in the clay prior to construction (not shown). Figure 10 indicates an initial under-drained porewater pressure profile within the shallower mudstone (104–123 m AOD) and hydrostatic pressures below a zero-pressure line at *c.* 120 m AOD in the deeper mudstone (below 104 m AOD). After excavation of the trial cutting, porewater pressures reduced most significantly at the middle and base of the shallower mudstone. This corresponds to zone (iii) in the shear-wave velocity profile in Figure 6. Smaller reductions of porewater pressure were measured near the excavated surface (zone (ii) in Fig. 6) and in the deeper mudstone (<104 m AOD). The porewater pressures measured near the excavated surface (115–123 m AOD) show greater scatter than at depth. They may have been influenced by ground disturbance during the excavation or the infiltration of ponded surface water during the wet autumn of 2019.

Figure 11 shows profiles of porewater pressure beneath the trial embankment with elevation for dates at the start of construction, the end of construction and following removal of the embankment. It shows hydrostatic porewater pressures throughout the ground profile that are in agreement with pre-construction measurements in the clay (Briggs *et al.* 2022). There were no piezometer measurements within the shallower mudstone (104–110 m AOD), so it was not possible to assess whether it was under-drained by the limestone, as it was below the trial cutting site. The porewater pressure profile was hydrostatic below 0.8 m bgl (121.2 m AOD). This is similar to the porewater pressure profile below 120 m AOD in the deeper mudstone beneath the trial cutting (Fig. 10). Porewater pressures increased during construction of the trial embankment at all elevations, and then reduced during removal of the embankment.

Figure 12 compares the changes in porewater pressures due to construction and removal of the earthworks with changes in the average total stresses calculated using equation (5). This uses porewater pressures measured at the end of construction of the trial cutting (*c.* 141 days) and at the end of construction of the trial

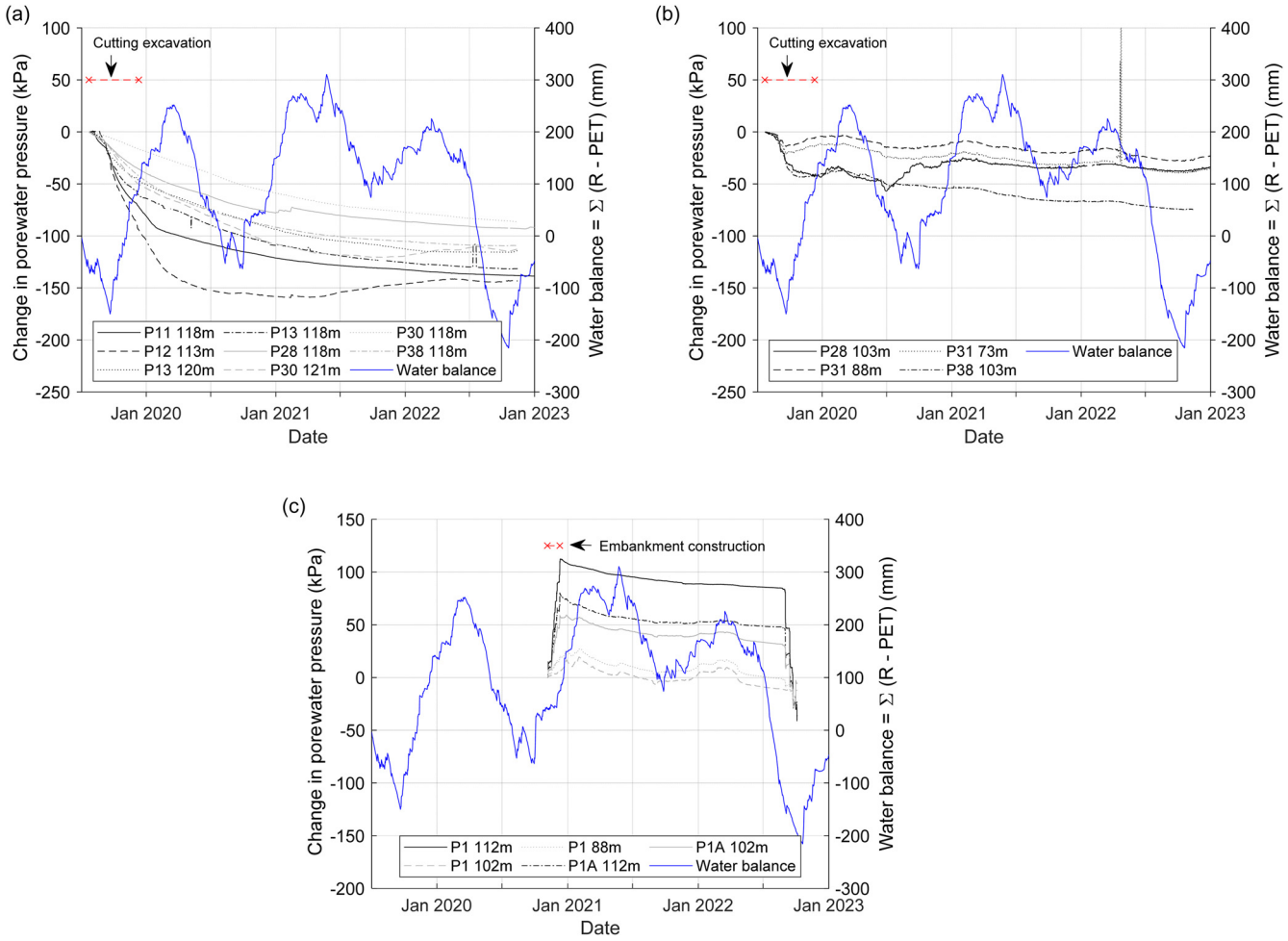


**Fig. 9.** Change in porewater pressure (kPa) since the start of earthwork construction compared to the water balance (mm) at Boddington. Piezometers are shown at: (**a**) locations beneath the trial cutting, at elevations above 104 m AOD; (**b**) locations beneath the trial cutting at elevations below 104 m AOD; and (**c**) locations beneath the trial embankment. The start and end dates for the earthwork construction are shown in red. The water balance (mm) is the sum of rainfall (*R*) minus potential evapotranspiration (PET).

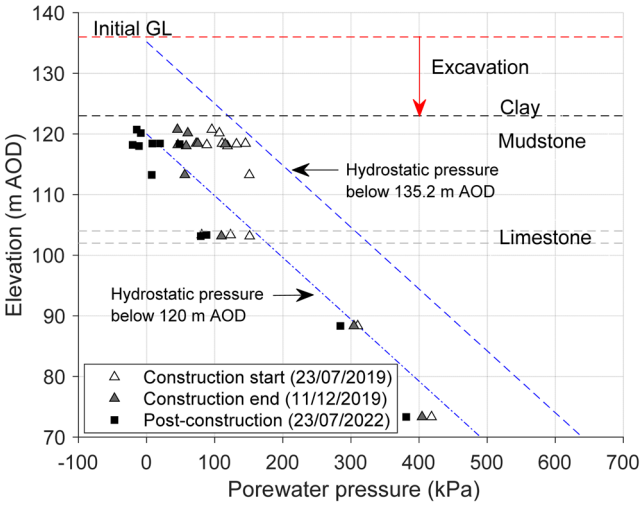


**Fig. 10.** Porewater pressures compared to the strata beneath the trial cutting. Porewater pressures are shown for the start of construction, the end of construction and post-construction. The initial ground level (GL) is shown in red. The depth of excavation (13 m) is shown by a red arrow. The hydrostatic pressures below 135.2 m AOD (0.8 m bgl) and 120 m AOD are shown in blue.

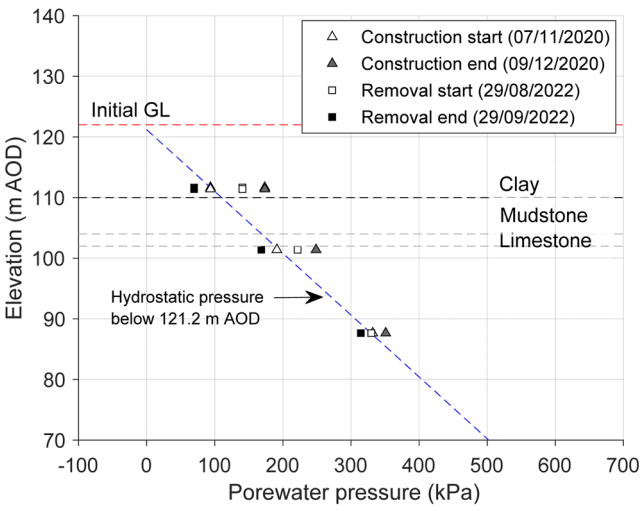


**Fig. 11.** Porewater pressures compared to the strata beneath the trial embankment. Porewater pressures are shown for the start of construction, the end of construction and removal. The initial ground level (GL) is shown in red. The hydrostatic pressure below 121.2 m AOD (0.8 mbgl) is shown in blue.


**Fig. 12.** The change in porewater pressure compared with change in the average total stress due to construction and removal of earthworks at each piezometer location. The dashed line shows a *B* ratio of unity.

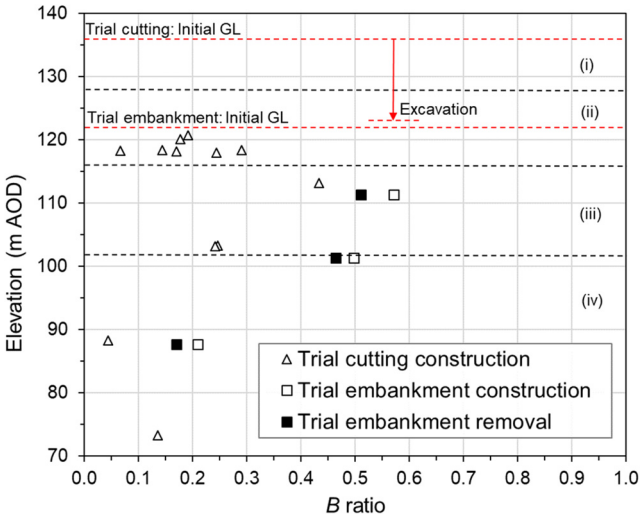


**Fig. 13.** The Skempton (1954) *B* ratio (equation 6) at each piezometer elevation calculated for: (**a**) the construction of the trial cutting; (**b**) construction of the trial embankment; and (**c**) removal of the trial embankment. The initial ground level (GL) at both sites is shown in red. The transition zones ((i)–(iv)) of changing stiffness identified in the shear-wave velocity profile (Fig. 6) are also shown.

embankment (*c*. 32 days). A line for a *B* ratio of unity is also shown. Figure 12 shows that the results from construction (loading) and removal (unloading) of the trial embankment are almost equal and opposite. They lie closer to the line of equality than the results from the construction of the trial cutting. The seven results for the trial cutting at $p \leq -250$ kPa are those from the shallower mudstone within the weathered clay and mudstone in zone (ii), shown in Figure 6. Consolidation analysis based on likely drainage path lengths (discussed later) shows that a significant dissipation of excess porewater pressure would have occurred before the end of construction at both the trial cutting and trial embankment (Fig. 9). Therefore, *B* values of less than unity would be expected, even in a fully saturated and relatively compressible soil. This is especially the case for the trial cutting, with its construction time of 141 days, and for piezometers at both sites that were located at the shallowest depths.

Figure 13 plots the calculated *B* values (equation 6) immediately after the construction and removal of the earthworks against the elevations of the piezometers. Beneath the trial cutting, the *B* values were generally less than 0.3 in the weathered clay and mudstone in zone (ii). In the mudstone (zones (iii) and (iv)) below, they reduced with elevation from a maximum value of 0.43 to 0.04. The *B* values directly beneath the trial embankment were 0.57 (at 113 m AOD). This was described as weathered clay in the borehole logs at the location of the embankment (Fig. 3) but corresponds to the elevation of zone (iii) in the shear-wave velocity profile from beneath the nearby trial cutting (Fig. 6). Lower *B* values ($B < 0.5$) are shown in the mudstone at lower elevations. At each elevation, the *B* values beneath the trial embankment were similar during construction (i.e. loading) and removal (i.e. unloading).

## Discussion

The porewater pressures in the clay and mudstone above 104 m AOD responded immediately to the construction of the earthworks (i.e. increased or decreased) but the magnitude of the change was less than the estimated change in average total stress. The *B* values were approximately 0.1–0.4 and 0.1–0.6 at the trial cutting and trial embankment, respectively. Porewater pressures in the mudstones located below the limestone (at 102–104 m AOD) were hydrostatic below a zero pressure line at *c*. 120–121 m AOD. They were relatively unresponsive to loading from the construction of earthworks at the ground surface.

At the trial cutting, the shallower mudstone above the limestone was initially under-drained by the strata below. Corresponding data were not available from beneath the trial embankment. Following construction, the porewater pressures at Boddington gradually reduced towards a new, lower equilibrium level. This new equilibrium level may reflect permanent changes to the ground and groundwater levels at the trial cutting (i.e. a 13 m lower elevation), which may also have influenced the trial embankment located directly downslope to the north of the cutting.

The observations at Boddington may be compared with those from a deep, staged, multi-propped excavation (Richards *et al.* 2007) in Upper Atherfield Clay and Lower Atherfield Clay (Greensand Group) strata under-drained by the more permeable Weald Clay (Wealden Group). Richards *et al.* (2007) showed that porewater pressures immediately reduced at each stage of construction and following reduction of the total stresses, with *B* values of between 0.67 and 0.77. New, reduced porewater pressure equilibrium conditions were reached in 4–15 weeks. This was the result of a short construction time and the result of passive, permanent drainage through a semi-permeable, contiguous piled wall, which created shorter drainage paths than at Boddington. Similar measurements in a deep, staged, multi-propped excavation in Gault Clay (Selbourne Group) showed immediate porewater pressure changes in the clay. The initial *B* values ranged between 0.5 and 0.75, increasing towards 0.9 as the level of the excavation approached the elevation of the piezometers (Ng 1998).

The *B* values measured by both Richards *et al.* (2007) and Ng (1998) were greater than those measured in the weathered clays and mudstones in zone (iii), above 104 m AOD, at Boddington. This could be partly due to the longer construction times at Boddington (and the longer period available for the dissipation of excess pore water pressures) and partly due to the cementation and greater stiffness of the mudstone, relative to the more compressible Atherfield Clay and Gault Clay. For example, the small-strain shear modulus ($G_0$) of the mudstone at Boddington is *c*. 350 MPa at 16 m bgl (Briggs *et al.* 2024). This is more than three times greater than the Gault Clay at the equivalent depth (*c*. 100 MPa: Ng *et al.* 1995) at the site described by Ng (1998). The high stiffness of the mudstone at Boddington makes the *B* values, even in truly undrained conditions, very sensitive to small reductions in the saturation ratio and the presence of pore air (Black and Lee 1973). Pore air could arise from the exsolution of dissolved gas during groundwater lowering (Powrie and Roberts 1990). Black and Lee

**Table 2.** Estimates of the saturated hydraulic conductivity of weathered clays and mudstones at shallow depth (>104 m AOD) beneath the trial cutting

| Scenario | $t$ (days) | $G_0$ (kPa) | $G_{0.1}$ (kPa) | $d$ (m) | $c_v$ ($m^2\ s^{-1}$) | $k_{sat}$ ($m\ s^{-1}$) |
|---|---|---|---|---|---|---|
| Vertical drainage, $k_{v,sat}$ | 1278 | $350 \times 10^3$ | $105 \times 10^3$ | 9.5 | $8.2 \times 10^{-7}$ | $2 \times 10^{-11}$ |
| Horizontal drainage, $k_{h,sat}$ | 1278 | $350 \times 10^3$ | $105 \times 10^3$ | 300 | $8.2 \times 10^{-4}$ | $2 \times 10^{-8}$ |

Scenarios are shown for a vertical drainage path and a horizontal drainage path.

(1973) showed that a reduction in the saturation ratio of just 0.5% from 100% (fully saturated) to 99.5% causes a reduction in the $B$ value from 1.0 to 0.2 in very stiff soils such as those at Boddington. This is confirmed by the calculation shown in Appendix A (equation A1). Thus, the low $B$ values at Boddington may be attributable to the high stiffness of the clays and mudstones in two respects: first, the direct impact of the stiffness in increasing the consolidation coefficient and reducing the timescale required for excess pore pressure dissipation; and, secondly, the resulting sensitivity to very small degrees of desaturation. The effects are seen especially in the $B$ values at shallow depth (*c*. 120 m AOD) beneath the trial cutting, where the reductions in mean total stress are greatest, the porewater pressures are lowest and the drainage pathway for excess porewater pressure dissipation during construction was shortest.

The results in Figure 9a show that porewater pressure dissipation was largely complete beneath the trial cutting by the end of the monitoring period (at time $t = 1278$ days). This was a more rapid reduction than was anticipated at the preliminary design stage (Menteth 2024). The effective coefficient of consolidation ($c_v$) can be estimated from $1 \approx c_v t/d^2$ (e.g. see Powrie 2018). For vertical drainage it is a lower bound because the drainage path length would have been greater than that associated with the final cutting geometry during the construction period, and unloading took place gradually over a period of 141 days rather than instantaneously at time $t = 0$. From the consolidation coefficient, the representative soil stiffness can be used to calculate the *in situ* saturated hydraulic conductivity, $k_{sat}$ ($m\ s^{-1}$), using one-dimensional consolidation theory:

$$k_{sat} = \frac{c_v \gamma_w}{E'_0} = \frac{c_v \gamma_w (1 - 2\nu')}{2G(1 - \nu')} \quad (7)$$

where $E'_0$ is the drained constrained modulus (kPa), $G$ is the shear modulus (kPa), $\gamma_w$ is the unit weight of water ($kN\ m^{-3}$) and Poisson's ratio ($\nu'$) is assumed to be 0.3 in effective stress terms (drained conditions). The *in situ* saturated hydraulic conductivity ($k_{sat}$) may be estimated for the vertical ($k_{v,sat}$) and horizontal ($k_{h,sat}$) directions, for given vertical ($d_v$) and horizontal ($d_h$) drainage path lengths. For vertical drainage, $k_{v,sat}$ is a lower bound because, during the 141 day construction period, the drainage path length would have been greater than that associated with the final cutting geometry.

Beneath the trial cutting, the 19 m-thick layer of clays and mudstones above the limestone (>104 m AOD) can drain upwards into the ground surface and downwards into the limestone below ($d_v$ of *c*. 9.5 m), or horizontally downslope and to the north ($d_h$ of *c*. 300 m). The small-strain shear modulus ($G_0$) of the clays and mudstones above the limestone at Boddington is *c*. 350 MPa, reducing to 30% of this value, $G_{0.1}$, at 0.1% strain (Briggs *et al.* 2024). Table 2 shows estimates of *in situ* saturated hydraulic conductivity in the vertical ($k_{v,sat}$) and horizontal ($k_{h,sat}$) directions based on these assumptions. Table 2 shows an estimated *in situ* $k_{v,sat}$ value of $2 \times 10^{-11}\ m\ s^{-1}$. This is approximately one order of magnitude lower than was measured in the triaxial permeability tests but one order of magnitude greater than was measured in the oedometer compression tests at depth (Fig. 5). Therefore, the estimate of *in situ* $k_{v,sat}$ is between those measured in the two types of laboratory test. This is reasonable given the difficulty of accurately assessing the hydraulic conductivity of low-permeability (Preene and Powrie 1993) or fissured soils (Rowe 1972), and that this is likely to be a lower-bound estimate for $k_{v,sat}$ below the trial cutting due to the assumed drainage path length. Table 2 shows that the estimated *in situ* $k_{h,sat}$ value of $2 \times 10^{-8}\ m\ s^{-1}$ is approximately two orders of magnitude lower than was measured in the *in situ* packer tests (Fig. 5), even assuming $d_h$ is *c*. 300 m. If the assumed drainage path length was reduced to a $d_h$ value of *c*. 30 m, the estimated *in situ* $k_{h,sat}$ value would reduce further to $2 \times 10^{-10}\ m\ s^{-1}$. Therefore, the estimated *in situ* $k_{h,sat}$ values are likely to be upper bounds that are still far less than those measured in the *in situ* packer tests. The estimates of $k_{v,sat}$ and $k_{h,sat}$ suggest that the dissipation of excess porewater pressures due to construction of the trial cutting, and the embankment, are most consistent with vertical drainage paths and the $k_{v,sat}$ values measured in laboratory tests.

## Conclusions

Porewater pressures in weathered clays and mudstones of the Charmouth Mudstone Formation (Lias Group) at Boddington, central England, were measured during the excavation of a 13 m-deep trial cutting and construction of an 8.2 m-high trial embankment. These were compared with ground investigation data and weather station measurements. The following conclusions can be drawn:

(1) Ground investigation data show a gradational weathering profile with depth in the clays and mudstones of the Charmouth Mudstone Formation. The clay near the ground surface is weathered, with weathered mudstone and unweathered mudstone below. A layer of calcareous siltstone (limestone) is located at *c*. 104 m AOD, below both the trial cutting and the trial embankment. The porewater pressures in the mudstone below the limestone were hydrostatic below *c*. 120 m AOD, at both the trial cutting and the trial embankment. The initial porewater pressure measurements (prior to construction) show that where the shallower mudstone is of significant thickness (e.g. it is 19 m thick beneath the cutting), it is under-drained by the underlying limestone. In terms of seasonal variations, the mudstone at elevations below 104 m AOD is isolated from the mudstone and clay layers above.

(2) Construction of the earthworks immediately affected the porewater pressures beneath both the trial cutting and the trial embankment. A consistent $B$ ratio was obtained for both the loading and unloading of the weathered clays and mudstones beneath the trial embankment. However, the $B$ ratios were lower than those reported from back-analyses of deep excavations in younger, more compressible overconsolidated clays and mudstones (Ng 1998; Richards *et al.* 2007). This may be explained by the construction times (30–140 days) being significant in comparison with the timescale of excess pore pressure dissipation, so that the construction and excavation processes were partly drained. The inferred higher values of consolidation coefficient are partly a result of the much greater stiffness of the clays and mudstones forming the Lias Group, compared with younger

and more clay-like geological deposits. This high stiffness also results in an increased sensitivity of the *B* value, even in genuinely undrained conditions, to very small degrees of desaturation (e.g. from 100% to 99.5% saturated) in stiff clays, as shown in laboratory tests (Black and Lee 1973) and in a calculation presented in Appendix A.

(3) The piezometer data show a reduction in long-term equilibrium porewater pressures beneath both the trial cutting and the trial embankment. This is the result of reductions in the surface load and groundwater lowering associated with excavation of the cutting. Long-term porewater pressure lowering is most evident in the weathered clay and mudstone strata above the limestone layer at 104 m AOD, at both the trial cutting and the trial embankment. An estimate of the *in situ* saturated hydraulic conductivity in the vertical ($k_{v,sat}$) and horizontal ($k_{h,sat}$) directions was compared with results from *in situ* and laboratory tests. This showed that excess porewater pressures generated beneath the trial cutting and the trial embankment during construction were likely to have dissipated along vertical drainage paths at a rate that was consistent with $k_{v,sat}$ values derived from laboratory tests.

*Scientific editing by Colin Serridge*

**Acknowledgements** The data were provided by HS2 Ltd. The authors are grateful to Dr Nicola Bicocchi, Mr Daniele Fornelli, the staff at Geotechnical Observations Ltd, COWI and EKFB; the late Prof. Lee Barbour and his colleagues at the University of Saskatchewan; and to the reviewers for their thoughtful comments and suggestions.

**Author contributions** **KMB**: data curation (equal) formal analysis (lead), methodology (lead), visualization (lead), writing – original draft (lead); **YTG**: data curation (equal), investigation (equal), writing – review & editing (supporting); **GJM**: formal analysis (supporting), methodology (supporting), writing – review & editing (supporting); **AR**: writing – review & editing (supporting); **WP**: formal analysis (supporting), supervision (equal), writing – review & editing (supporting); **SB**: writing – review & editing (supporting); **NS**: supervision (equal), writing – review & editing (supporting).

**Funding** This work was funded by the Engineering and Physical Sciences Research Council (grant No. EP/R034575/1 awarded to K.M. Briggs and W. Powrie) and the Royal Academy of Engineering (grant No. RCSRF1920\10 \65 awarded to K.M. Briggs).

**Competing interests** The authors declare that they have no known competing financial interests or personal relationships that could have appeared to influence the work reported in this paper.

**Data availability** The data presented in this paper are available online via the University of Bath institutional repository (Briggs 2024) and may be accessed at https://doi.org/10.15125/BATH-01380

## Appendix A

Skempton's (1954) *B* value can be very sensitive to the saturation ratio in very stiff soils (Black and Lee 1973). It can be calculated by considering the bulk stiffness of the soil ($K$), the bulk stiffness of water ($K_w \approx 2.2$ GPa), the soil porosity ($n$) and the saturation ratio ($S$). A bulk stiffness for the air can be assumed to be equal to the pore pressure at atmospheric pressure ($u_{atm} = 100$ kPa) using the ideal gas law, or equal to the atmospheric pressure plus the porewater pressure ($u$) beneath the earthworks. The bulk stiffness of the soil ($K$) can be derived from the small-strain shear modulus ($G_0$) and drained Poisson's ratio ($\nu'$) from $K' = 2G_0(1+\nu')/3(1-2\nu')$. The *B* value that considers the stiffness and volumetric strain of the soil, water and air phases can be derived from first principles as:

$$B = \frac{1}{1 + (nSK'/K_w) + (n(1-S)K'/u + u_{atm})} \quad \text{(A1)}$$

The *B* values calculated using equation (A1) for high saturation ratios (0.98–1) are shown in Figure A1. They were calculated using assumed material properties for the Charmouth Mudstone Formation (Briggs *et al.* 2022; 2024) and the pore pressures measured at 113 m AOD beneath the trial cutting and the trial embankment (Figs 10, 11). Figure A1 shows that for a small reduction in saturation ratio to 0.995 (i.e. 99.5% saturation) the *B* value can reduce to 0.2 for pore pressures at the end of construction for the trial embankment and after removal of the trial embankment. Owing to the higher pore pressures beneath the trial embankment,

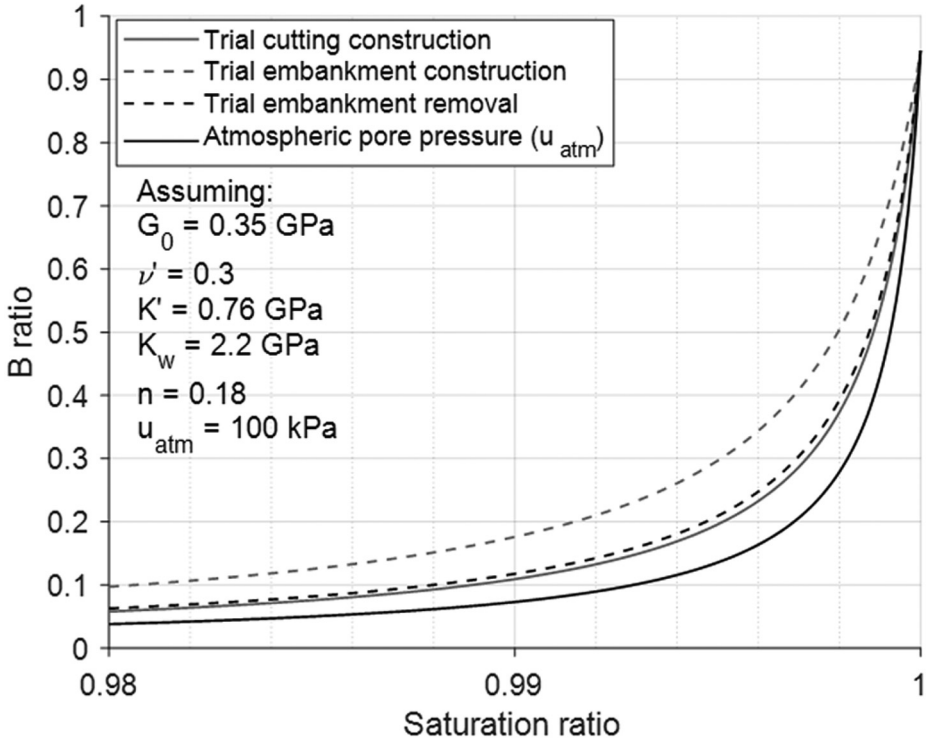


**Fig. A1.** The calculated variation of the *B* ratio at high saturation ratios (0.98–1) for pore (water and air) pressures at 113 m AOD beneath the trial cutting and trial embankment after construction and removal. Assumed values are shown for the small-strain shear modulus ($G_0$), drained Poisson's ratio ($\nu'$), drained bulk modulus ($K'$), bulk modulus of water ($K_w$), porosity ($n$) and atmospheric pressure ($u_{atm}$).

the $B$ value reduces to 0.3 at the same saturation ratio. Therefore, the $B$ values beneath the trial embankment after construction are slightly less sensitive to desaturation than those beneath the trial cutting after construction or those beneath the trial embankment after removal.

## References


Black, D.K. and Lee, K.L. 1973. Saturating laboratory samples by back pressure. *Journal of the Soil Mechanics and Foundations Division*, **99**, 75–93, https://doi.org/10.1061/JSFEAQ.0001847

Blight, G.E. 1997. Interactions between the atmosphere and the Earth. *Géotechnique*, **47**, 715–767, https://doi.org/10.1680/geot.1997.47.4.713

Booth, S., Merritt, J. and Rose, J. 2015. Quaternary Provinces and Domains – a quantitative and qualitative description of British landscape types. *Proceedings of the Geologists' Association*, **126**, 163–187, https://doi.org/10.1016/j.pgeola.2014.11.002

Bormann, H. 2011. Sensitivity analysis of 18 different potential evapotranspiration models to observed climatic change at German climate stations. *Climatic Change*, **104**, 729–753, https://doi.org/10.1007/s10584-010-9869-7

Briggs, K. 2024. *Pore Water Pressure Measurements from a Trial Cutting and Trial Embankment at Boddington*. University of Bath Research Data Archive, Bath, UK, https://doi.org/10.15125/BATH-01380

Briggs, K., Trinidad Gonzalez, Y., Meijer, G.J., Powrie, W., Butler, S. and Sartain, N. 2024. In-situ characterization of strength and stiffness in a weathered mudstone profile. *In*: *Proceedings of the 7th International Conference on Geotechnical and Geophysical Site Characterization, 18–21 June 2024, Barcelona*, https://www.scipedia.com/public/Briggs*_et_al_2024a

Briggs, K.M., Smethurst, J.A., Powrie, W. and O'Brien, A.S. 2016. The influence of tree root water uptake on the long term hydrology of a clay fill railway embankment. *Transportation Geotechnics*, **9**, 31–48, https://doi.org/10.1016/j.trgeo.2016.06.001

Briggs, K.M., Blackmore, L. *et al.* 2022. The influence of weathering on index properties and undrained shear strength for the Charmouth Mudstone Formation of the Lias Group at a site near Banbury, Oxfordshire, UK. *Quarterly Journal of Engineering Geology and Hydrogeology*, **55**, https://doi.org/10.1144/qjegh2021-066

BSI 2012. *BS EN ISO 22282-3:2012: Geotechnical Investigation and Testing – Geohydraulic Testing. Part 3: Water Pressure Tests in Rock*. British Standards Institution (BSI), London.

BSI 2017. *BS EN ISO 17892-5:2017: Geotechnical Investigation and Testing. Laboratory Testing of Soil. Incremental Loading Oedometer Test. Part 5: Incremental Loading Oedometer Test*. British Standards Institution (BSI), London.

BSI 2019. *BS EN ISO 17892-11:2019: Geotechnical Investigation and Testing. Laboratory Testing of Soil. Permeability Tests. Part 11: Permeability Tests*. British Standards Institution (BSI), London.

BSI 2021. *BS EN ISO 18674-4:2020 Geotechnical Investigation and Testing – Geotechnical Monitoring by Field Instrumentation. Measurement of Pore Water Pressure: Piezometers*. British Standards Institution (BSI), London.

Environment Agency 2024. Hydrology Data Explorer. Environment Agency, Department for Environment Food & Rural Affairs (Defra), London, https://environment.data.gov.uk/hydrology/station/95a49ba1-69ed-4d52-8489-e6793fe88c68

Gibson, S.M., Bateman, M.D., Murton, J.B., Barrows, T.T., Fifield, L.K. and Gibbard, P.L. 2022. Timing and dynamics of Late Wolstonian Substage 'Moreton Stadial' (MIS 6) glaciation in the English West Midlands, UK. *Royal Society Open Science*, **9**, https://doi.org/10.1098/rsos.220312

Gray, H. 1936. Stress distribution in elastic solids. *In*: Casagrande, A., Rutledge, P.C. and Watson, J.D. (eds) *Proceedings of the International Conference on Soil Mechanics and Foundation Engineering, June 22–26, 1936, Volume 2*. Harvard University Graduate School of Engineering, Cambridge, MA, 157–168.

Hobbs, P.R.N., Entwisle, D.C. *et al.* 2012. *Engineering Geology of British Rocks and Soils: Lias Group*. British Geological Survey Internal Report OR/12/032. British Geological Survey, Keyworth, Nottingham, UK.

Lawrence, U., Menkiti, C.O. and Black, M. 2018*a*. Regional-scale groundwater investigations for the Crossrail project. *Quarterly Journal of Engineering Geology and Hydrogeology*, **51**, 31–37, https://doi.org/10.1144/qjegh2016-047

Lawrence, U., Menkiti, C.O. and Black, M. 2018*b*. Groundwater monitoring of the deep aquifer for the construction phase of the Crossrail project. *Quarterly Journal of Engineering Geology and Hydrogeology*, **51**, 38–48, https://doi.org/10.1144/qjegh2016-046

Menteth, T. 2024. Rail: How HS2's earthworks trials have led to major carbon savings. *Ground Engineering*, January 2024, 14–16, https://www.geplus.co.uk/features/rail-how-hs2s-earthworks-trials-have-led-to-major-carbon-savings-23-01-2024/

Met Office. 2024*a*. *2019: A Year in Review*. Met Office, Exeter, UK, https://www.metoffice.gov.uk/about-us/press-office/news/weather-and-climate/2019/weather-overview-2019

Met Office. 2024*b*. *UK Climate Averages*. Met Office, Exeter, UK, https://www.metoffice.gov.uk/research/climate/maps-and-data/uk-climate-averages/gcqbgxb2n

Newman, T. 2009. The impact of adverse geological conditions on the design and construction of the Thames Water Ring Main in Greater London, UK. *Quarterly Journal of Engineering Geology and Hydrogeology*, **42**, 5–20, https://doi.org/10.1144/1470-9236/08-035

Ng, C.W. 1998. Observed performance of multipropped excavation in stiff clay. *Journal of Geotechnical and Geoenvironmental Engineering*, **124**, 889–905, https://doi.org/10.1061/(ASCE)1090-0241(1998)124:9(889)

Ng, C., Bolton, M. and Dasari, G. 1995. The small strain stiffness of a carbonate stiff clay. *Soils and Foundations*, **35**, 109–114, https://doi.org/10.3208/sandf.35.4_109

Peck, R.B. 1969. Advantages and limitations of the observational method in applied soil mechanics. *Géotechnique*, **19**, 171–187, https://doi.org/10.1680/geot.1969.19.2.171

Poulos, H.G. 2022. Use of shear wave velocity for foundation design. *Geotechnical and Geological Engineering*, **40**, 1921–1938, https://doi.org/10.1007/s10706-021-02000-w

Poulos, H.G. and Davis, E.H. 1974. *Elastic Solutions for Soil and Rock Mechanics*. John Wiley & Sons, New York.

Powderham, A. and O'Brien, A. 2020. *The Observational Method in Civil Engineering: Minimising Risk, Maximising Economy*. CRC Press, London.

Powrie, W. 2018. *Soil Mechanics: Concepts and Applications*. CRC Press, London.

Powrie, W. and Roberts, T.O.L. 1990. Field trial of an ejector well dewatering system at Conwy, North Wales. *Quarterly Journal of Engineering Geology, London*, **23**, 169–185, https://doi.org/10.1144/GSL.QJEG.1990.023.02.06

Powrie, W. and Roberts, T.O.L. 1995. Case history of a dewatering and recharge system in chalk. *Géotechnique*, **45**, 599–609, https://doi.org/10.1680/geot.1995.45.4.599

Preene, M. 2019. Design and interpretation of packer permeability tests for geotechnical purposes. *Quarterly Journal of Engineering Geology and Hydrogeology*, **52**, 182–200, https://doi.org/10.1144/qjegh2018-079

Preene, M. and Powrie, W. 1993. Steady-state performance of construction dewatering systems in fine soils. *Géotechnique*, **43**, 191–205, https://doi.org/10.1680/geot.1993.43.2.191

Richards, D.J., Powrie, W., Roscoe, H. and Clark, J. 2007. Pore water pressure and horizontal stress changes measured during construction of a contiguous bored pile multi-propped retaining wall in Lower Cretaceous clays. *Géotechnique*, **57**, 197–205, https://doi.org/10.1680/geot.2007.57.2.197

Ridley, A.M., Dineen, K., Burland, J.B. and Vaughan, P.R. 2003. Soil matrix suction: some examples of its measurement and application in geotechnical engineering. *Géotechnique*, **53**, 241–253, https://doi.org/10.1680/geot.2003.53.2.241

Roberts, T.O.L. and Preene, M. 1994. The design of groundwater control systems using the observational method. *Géotechnique*, **44**, 727–734, https://doi.org/10.1680/geot.1994.44.4.727

Roberts, T.O.L., Roscoe, H., Powrie, W. and Butcher, D.J. 2007. Controlling clay pore pressures for cut-and-cover tunnelling. *Proceedings of the Institution of Civil Engineers – Geotechnical Engineering*, **160**, 227–236, https://doi.org/10.1680/geng.2007.160.4.227

Rowe, P.W. 1972. The relevance of soil fabric to site investigation practice. *Géotechnique*, **22**, 195–300, https://doi.org/10.1680/geot.1972.22.2.195

Schendel, U. 1967. Vegetationswasserverbrauch und -wasserbedarf. *Habilitation, Kiel*, **137**, 1–11.

Skempton, A.W. 1954. The pore-pressure coefficients $A$ and $B$. *Géotechnique*, **4**, 143–147, https://doi.org/10.1680/geot.1954.4.4.143

Smethurst, J.A., Clarke, D. and Powrie, W. 2006. Seasonal changes in pore water pressure in a grass-covered cut slope in London Clay. *Géotechnique*, **56**, 523–537, https://doi.org/10.1680/geot.2006.56.8.523

Tarantino, A., Ridley, A.M. and Toll, D.G. 2008. Field measurement of suction, water content, and water permeability. *Geotechnical and Geological Engineering*, **26**, 751–782, https://doi.org/10.1007/s10706-008-9205-4

Vardanega, P.J. and Bolton, M.D. 2013. Stiffness of clays and silts: normalizing shear modulus and shear strain. *Journal of Geotechnical and Geoenvironmental Engineering*, **139**, 1575–1589, https://doi.org/10.1061/(ASCE)GT.1943-5606.0000887

Vaughan, P.R. and Walbancke, H.J. 1973. Pore pressure changes and the delayed failure of cutting slopes in overconsolidated clay. *Géotechnique*, **23**, 531–539, https://doi.org/10.1680/geot.1973.23.4.531

Wan, M.S. and Standing, J.R. 2014. Field measurement by fully grouted vibrating wire piezometers. *Proceedings of the Institution of Civil Engineers – Geotechnical Engineering*, **167**, 547–564, https://doi.org/10.1680/geng.13.00153

Whittle, A.J., Hashash, Y.M. and Whitman, R.V. 1993. Analysis of deep excavation in Boston. *Journal of Geotechnical Engineering*, **119**, 69–90, https://doi.org/10.1061/(ASCE)0733-9410(1993)119:1(69)